Full Wave Network Representation for Rectangular, Circular, and Elliptical to Elliptical Waveguide Junctions

Benito Gimeno and Marco Guglielmi

***Abstract*—In this paper, two contributions to the study of the elliptical waveguides are given: an efficient technique to obtain the modal spectrum for elliptical waveguides and the analysis of the junctions between rectangular, circular, or elliptical to elliptical waveguides. In addition to theoretical results, experimental results are also presented finding good agreement between prediction and measurement.**

I. Introduction

ELLIPTICAL waveguides have already been studied in the past and a number of contributions can be found in the technical literature investigating their modal structure [1]–[12], or simple step junctions [13]. In this paper, the authors give two contributions to the study of elliptical waveguides. First, the authors develop a computationally efficient approach to obtain the modal spectrum in elliptical waveguide regions to avoid the slow convergence of the Mathieu functions. Second, the authors analyze the junctions between rectangular, circular, or elliptical and elliptical waveguide.

The technique used for the modal analysis is based on the transformation of the Helmholtz equation in elliptical coordinates into an equivalent linear matrix eigenvalue problem by means of the Galerkin method [14]–[16]. The second part of the paper is devoted to the study of junctions from rectangular, circular, or elliptical to elliptical waveguides [17]. The convergence of the method is analyzed, showing good behavior. Finally, theoretical results are compared with measurements finding a good agreement.

II. Modal Analysis of Elliptical Waveguides

The analytical expressions of the vector mode functions for an elliptical waveguide can be found in the technical literature in terms of the Mathieu functions [18]. However, the computation of these functions using standard routines can result in long central processing unit (CPU) time. Therefore, in this paper the authors have chosen an alternative procedure in order to obtain codes which are computationally more efficient.

From a mathematical point of view, an ellipse is characterized by the major and minor semi-axis, denoted as a and b, respectively. Other relevant parameters are the focal semi-distance given by $c = \sqrt{a^2 - b^2}$, and the eccentricity of the ellipse given by $e = c/a$. The elliptical coordinate system is defined as the intersection of two families of confocal ellipses and confocal hyperbolas [19]. Each intersection point corresponds to a point defined by the coordinates $x = c(\cosh \xi)(\cos \eta)$, $y = c(\sinh \xi)(\sin \eta)$, where ξ is the radial elliptical coordinate, and η is the angular elliptical coordinate. The coordinate η varies from 0 to 2π, and the coordinate ξ varies from 0 to $\xi_0 = \operatorname{arccosh}(1/e)$. Finally, $\mathbf{u}_\xi$ and $\mathbf{u}_\eta$ represent the unitary vectors associated with the coordinates ξ and η, respectively.

The authors start our derivation by writing the Helmholtz equation in elliptical coordinates

$$\left[\frac{2}{c^2(\cosh 2\xi - \cos 2\eta)}\left(\frac{\partial^2}{\partial \xi^2} + \frac{\partial^2}{\partial \eta^2}\right) + k_{t_m}^2\right]\Psi_m(\xi, \eta) = 0 \tag{1}$$

where k_{t_m} is the transverse wavenumber of the mth mode, and the potential $\Psi_m(\xi, \eta)$ represents the axial electric or magnetic component for the mth TM or TE modes, respectively. The longitudinal propagation constant is given by

$$\beta_m^2 = \omega^2 \mu \varepsilon - k_{t_m}^2. \tag{2}$$

In the classical modal analysis, the method of separation of variables is used thus leading to Mathieu functions. To increase the computational efficiency, the authors first rewrite (1) as an eigenvalue equation

$$\begin{aligned}\mathcal{L}\Psi_m(\xi, \eta) \equiv &\left[\frac{2}{c^2(\cosh 2\xi - \cos 2\eta)}\left(\frac{\partial^2}{\partial \xi^2} + \frac{\partial^2}{\partial \eta^2}\right)\right] \\ &\cdot \Psi_m(\xi, \eta) \\ = &-k_{t_m}^2 \Psi_m(\xi, \eta)\end{aligned} \tag{3}$$

where $\mathcal{L}$ is a linear differential operator. Next, the authors write $\Psi_m(\xi, \eta)$ in the form

$$\Psi_m(\xi, \eta) = \sum_{i=1}^{N} d_i^{(m)} \alpha_i(\xi, \eta) \tag{4}$$

being $d_i^{(m)}$ unknown expansion coefficients, and $\alpha_i(\xi, \eta)$ a set of basis functions which directly satisfy the Dirichlet or Neumann boundary conditions, for TM or TE modes, respectively. Next, following the Galerkin method, the authors

Manuscript received February 16, 1996; revised November 21, 1996.

B. Gimeno is with the Departamento de Fisica Aplicada, Universidad de Valencia, 46100 Burjasot (Valencia) Spain.

M. Guglielmi is with the European Space Research and Technology Centre (ESTEC), 2200 AG Noordwijk, The Netherlands.

Publisher Item Identifier S 0018-9480(97)01709-2.

0018–9480/97$10.00 © 1997 IEEE

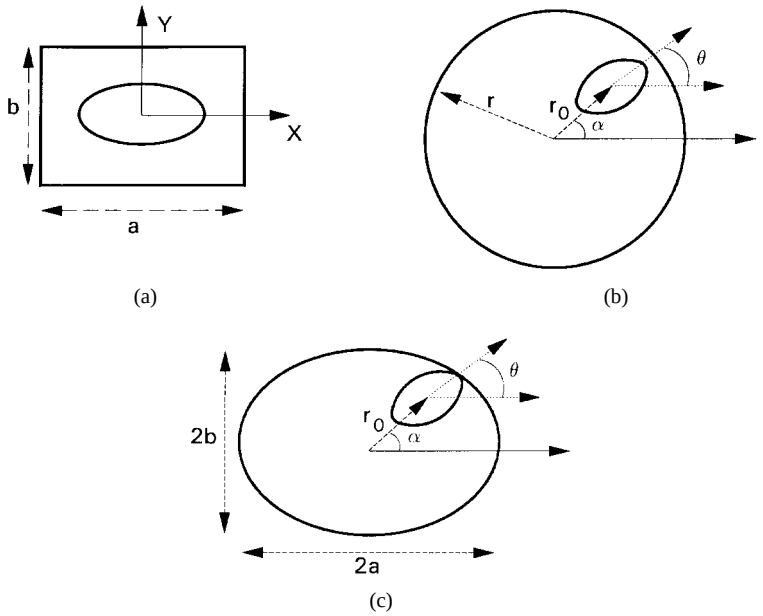

Fig. 1. Geometries of the junctions studied in this paper: (a) rectangular to elliptical junction, (b) circular to elliptical junction, and (c) elliptical to elliptical junction.

insert (4) into (3), obtaining

$$\sum_{i=1}^{N} d_i^{(m)} \mathcal{L}\alpha_i(\xi, \eta) = -k_{t_m}^2 \sum_{i=1}^{N} d_i^{(m)} \alpha_i(\xi, \eta) \tag{5}$$

so that, multiplying by $\alpha_j(\xi, \eta)$ and integrating both sides of (5), the authors finally write

$$\sum_{i=1}^{N} d_i^{(m)} \langle \mathcal{L}\alpha_i | \alpha_j \rangle = -k_{t_m}^2 \sum_{i=1}^{N} d_i^{(m)} \langle \alpha_i | \alpha_j \rangle, \quad j = 1, 2, \cdots, N \tag{6}$$

where the symbol $\langle | \rangle$ indicates

$$\langle f | g \rangle = \frac{c^2}{2} \int_0^{2\pi} \int_0^{\xi_0} (\cosh 2\xi - \cos 2\eta) \cdot f(\xi, \eta) g^*(\xi, \eta)\, d\eta\, d\xi \tag{7}$$

Equation (1) has therefore successfully been transformed into the linear matrix eigenvalue system in (6). Now, using the original notation of [14], the authors rewrite (6) as follows

$$\underline{\underline{P}}\, \underline{D^{(m)}} = k_{t_m}^2\, \underline{\underline{Q}}\, \underline{D^{(m)}} \tag{8}$$

where the elements of the matrices $\underline{\underline{P}}$, $\underline{\underline{Q}}$, and $\underline{D^{(m)}}$ are given by

$$\begin{aligned} Q_{ij} &= \langle \alpha_i | \alpha_j \rangle, && i, j = 1, 2, \cdots, N \\ P_{ij} &= -\langle \mathcal{L}\alpha_i | \alpha_j \rangle, && i, j = 1, 2, \cdots, N \\ D_i^{(m)} &= d_i^{(m)}, && i = 1, 2, \cdots, N \end{aligned} \tag{9}$$

The linear eigenvalue problem obtained can be easily solved with standard mathematical subroutines for matrix operations, obtaining the transverse wavenumbers $k_{t_m}^2$ and the expansion coefficients $d_i^{(m)}$ of each mode. Finally, the vector mode functions obtained are normalized according to

$$\begin{aligned} \langle \mathbf{e}_m, \mathbf{e}_n \rangle &= \int_{CS} \mathbf{e}_m \mathbf{e}_n^*\, dS = \delta_{m,n} \\ \langle \mathbf{h}_m, \mathbf{h}_n \rangle &= \int_{CS} \mathbf{h}_m \mathbf{h}_n^*\, dS = \delta_{m,n} \end{aligned} \tag{10}$$

where $\delta_{m,n}$ is the Dirac delta function, and CS is the waveguide cross section. The derivation up to this point is general. The application to TM and TE polarizations requires some further analytical developments.

A. TM Modes

There are two families of TM modes, denoted as TM_e and TM_o, corresponding to the even and odd solutions of the Mathieu functions [18], respectively. The basis functions chosen are

$$\alpha_i^{\mathrm{TM}_e}(\xi, \eta) = \cos\left[\left(r + \frac{1}{2}\right)\pi \frac{\xi}{\xi_0}\right] \cos(s\eta) \tag{11}$$

$$\alpha_i^{\mathrm{TM}_o}(\xi, \eta) = \sin\left(r\pi \frac{\xi}{\xi_0}\right) \sin(s\eta) \tag{12}$$

where the index i corresponds to the pairs of integers (r, s). The axial electric component then becomes

$$\begin{aligned} E_{z_m}^{\mathrm{TM}_e}(\xi, \eta) &= \sum_{r=0}^{N_r-1} \sum_{s=0}^{N_s-1} d_{rs}^{\mathrm{TM}_e,(m)} \cdot \cos\left[\left(r + \frac{1}{2}\right)\pi \frac{\xi}{\xi_0}\right] \cos(s\eta) \\ &\equiv \sum_{i=1}^{N} d_i^{\mathrm{TM}_e,(m)} \alpha_i^{\mathrm{TM}_e}(\xi, \eta) \end{aligned} \tag{13}$$

$$\begin{aligned} E_{z_m}^{\mathrm{TM}_o}(\xi, \eta) &= \sum_{r=1}^{N_r} \sum_{s=1}^{N_s} d_{rs}^{\mathrm{TM}_o,(m)} \sin\left(r\pi \frac{\xi}{\xi_0}\right) \sin(s\eta) \\ &\equiv \sum_{i=1}^{N} d_i^{\mathrm{TM}_o,(m)} \alpha_i^{\mathrm{TM}_o}(\xi, \eta) \end{aligned} \tag{14}$$

where $N = N_r \times N_s$ is the total number of terms. The specific choice of the analytical form in (11) and (12) has been dictated by the Dirichlet boundary conditions, namely

$$E_{z_m}^{\mathrm{TM}_e}(\xi, \eta)|_{\xi=\xi_0} = E_{z_m}^{\mathrm{TM}_o}(\xi, \eta)|_{\xi=\xi_0} = 0 \tag{15}$$

The elements of the matrices $\underline{\underline{P}}$ and $\underline{\underline{Q}}$ are easily obtained, resulting in the very simple expressions

$$\begin{aligned} Q_{ij}^{\mathrm{TM}_e} &= I_{r,t}^{(c1)} \frac{\pi c^2}{\epsilon_s} \delta_{s,p} - I_{s,p}^{(c2)} \frac{c^2 \xi_0}{4} \delta_{r,t} \\ P_{ij}^{\mathrm{TM}_e} &= \left[\frac{\pi^3}{\epsilon_s \xi_0} \left(r + \frac{1}{2}\right)\left(t + \frac{1}{2}\right) + \frac{\xi_0 \pi}{2}(\epsilon_s - 1)\, sp \right] \\ &\quad \cdot \delta_{s,p}\delta_{r,t} \qquad i \equiv (r, s), \quad j \equiv (t, p) \end{aligned} \tag{16}$$

$$\begin{aligned} Q_{ij}^{\mathrm{TM}_o} &= I_{r,t}^{(s1)} \frac{\pi c^2}{2} \delta_{s,p} - I_{s,p}^{(s2)} \frac{c^2 \xi_0}{4} \delta_{r,t} \\ P_{ij}^{\mathrm{TM}_o} &= \left(\frac{\pi^3}{2\xi_0} rt + \frac{\xi_0 \pi}{2} sp \right) \delta_{s,p}\delta_{r,t}, \quad i \equiv (r, s), \quad j \equiv (t, p) \end{aligned} \tag{17}$$

where $\epsilon_s = 1$ if $s = 0$, $\epsilon_s = 2$ if $s \neq 0$, and the expressions for $I_{r,t}^{(c1)}$, $I_{s,p}^{(c2)}$, $I_{r,t}^{(s1)}$, and $I_{s,p}^{(s2)}$ are given in Appendix I.

The authors can now write the analytical expressions of the scalar potentials $\varphi_m^{\mathrm{TM}_e}$ and $\varphi_m^{\mathrm{TM}_o}$ in the form

$$\begin{aligned} \varphi_m^{\mathrm{TM}_e}(\xi, \eta) &= \mathcal{N}_m^{\mathrm{TM}_e} \sum_{r=0}^{N_r-1} \sum_{s=0}^{N_s-1} d_{rs}^{\mathrm{TM}_e, (m)} \\ &\quad \cdot \cos\left[\left(r + \frac{1}{2}\right) \pi \frac{\xi}{\xi_0} \right] \cos(s\eta) \end{aligned} \tag{18}$$

$$\begin{aligned} \varphi_m^{\mathrm{TM}_o}(\xi, \eta) &= \mathcal{N}_m^{\mathrm{TM}_o} \sum_{r=1}^{N_r} \sum_{s=1}^{N_s} d_{rs}^{\mathrm{TM}_o, (m)} \\ &\quad \cdot \sin\left(r\pi \frac{\xi}{\xi_0} \right) \sin(s\eta) \end{aligned} \tag{19}$$

where $\mathcal{N}_m^{\mathrm{TM}_e}$ and $\mathcal{N}_m^{\mathrm{TM}_o}$, the normalization factors according to the normalization condition in (10), are given by

$$\begin{aligned} \mathcal{N}_m^{\mathrm{TM}_e} &= \left\{ \frac{\xi_0 \pi}{2} \sum_{r=0}^{N_r-1} \sum_{s=0}^{N_s-1} [d_{rs}^{\mathrm{TM}_e, (m)}]^2 \right. \\ &\quad \left. \cdot \left[\left(r + \frac{1}{2}\right)^2 \frac{2}{\epsilon_s} \left(\frac{\pi}{\xi_0}\right)^2 + s^2(\epsilon_s - 1) \right] \right\}^{-1/2} \end{aligned} \tag{20}$$

$$\mathcal{N}_m^{\mathrm{TM}_o} = \left\{ \frac{\xi_0 \pi}{2} \sum_{r=1}^{N_r} \sum_{s=1}^{N_s} [d_{rs}^{\mathrm{TM}_o, (m)}]^2 \cdot \left[r^2 \left(\frac{\pi}{\xi_0}\right)^2 + s^2 \right] \right\}^{-1/2} \tag{21}$$

so that the authors can finally write for the TM vector mode functions the following expressions

$$\begin{aligned} \mathbf{e}_m^{\mathrm{TM}_\alpha} &= \nabla_t \varphi_m^{\mathrm{TM}_\alpha} \\ \mathbf{h}_m^{\mathrm{TM}_\alpha} &= \mathbf{u}_z \times \nabla_t \varphi_m^{\mathrm{TM}_\alpha} \qquad \alpha = e, o \end{aligned} \tag{22}$$

where ∇_t is the transverse nabla operator. Finally, the modal admittance of the TM modes is given by

$$Y_m^{\mathrm{TM}} = \frac{\omega \varepsilon}{\beta_m^{\mathrm{TM}}} \tag{23}$$

where β_m^{TM} is the propagation constant given in (2).

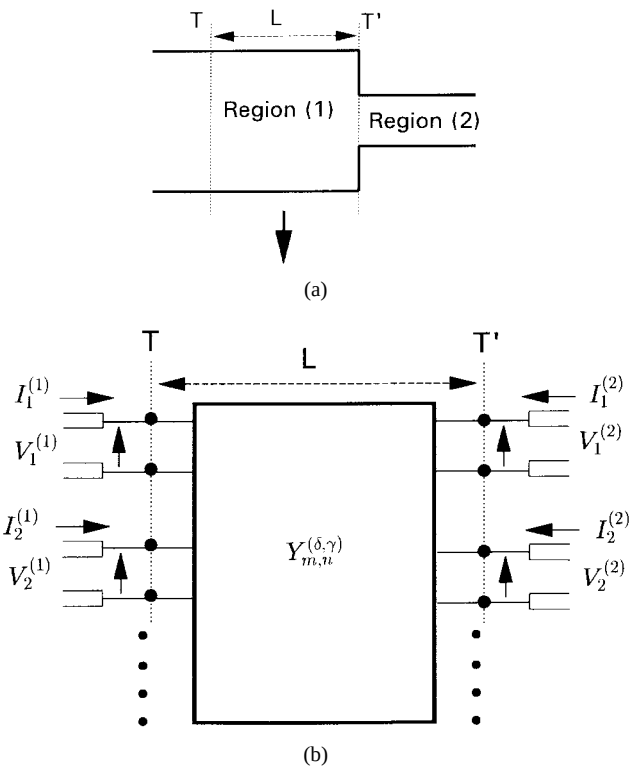

Fig. 2. Junction from a rectangular, circular, or elliptical waveguide [denoted as region (1)] to a elliptical waveguide [denoted as region (2)]. The multimode equivalent network representation of the junction is also shown.

B. TE Modes

The same procedure has been applied for TE modes, so the authors omit the details. The basis functions chosen are

$$\alpha_i^{\mathrm{TE}_e}(\xi, \eta) = \cos\left(r\pi \frac{\xi}{\xi_0} \right) \cos(s\eta) \tag{24}$$

$$\alpha_i^{\mathrm{TE}_o}(\xi, \eta) = \sin\left[\left(r + \frac{1}{2}\right) \pi \frac{\xi}{\xi_0} \right] \sin(s\eta) \tag{25}$$

where the index i corresponds to the pairs of integers (r, s). The axial magnetic component becomes

$$\begin{aligned} H_{z_m}^{\mathrm{TE}_e}(\xi, \eta) &= \sum_{r=0}^{N_r-1} \sum_{s=0}^{N_s-1} d_{rs}^{\mathrm{TE}_e, (m)} \cdot \cos\left(r\pi \frac{\xi}{\xi_0} \right) \cos(s\eta) \\ &\equiv \sum_{i=1}^{N} d_i^{\mathrm{TE}_e, (m)} \alpha_i^{\mathrm{TE}_e}(\xi, \eta) \\ &\quad (r = s = 0 \text{ is not considered}) \end{aligned} \tag{26}$$

$$\begin{aligned} H_{z_m}^{\mathrm{TE}_o}(\xi, \eta) &= \sum_{r=0}^{N_r-1} \sum_{s=1}^{N_s} d_{rs}^{\mathrm{TE}_o, (m)} \sin\left[\left(r + \frac{1}{2}\right) \pi \frac{\xi}{\xi_0} \right] \sin(s\eta) \\ &\equiv \sum_{i=1}^{N} d_i^{\mathrm{TE}_o, (m)} \alpha_i^{\mathrm{TE}_o}(\xi, \eta). \end{aligned} \tag{27}$$

The specific choice of the analytical form in (24) and (25) has been imposed by the Neumann boundary conditions, namely

$$\frac{\partial}{\partial \xi} H_{z_m}^{\mathrm{TM}_e}(\xi, \eta)|_{\xi=\xi_0} = \frac{\partial}{\partial \xi} H_{z_m}^{\mathrm{TM}_o}(\xi, \eta)|_{\xi=\xi_0} = 0. \tag{28}$$

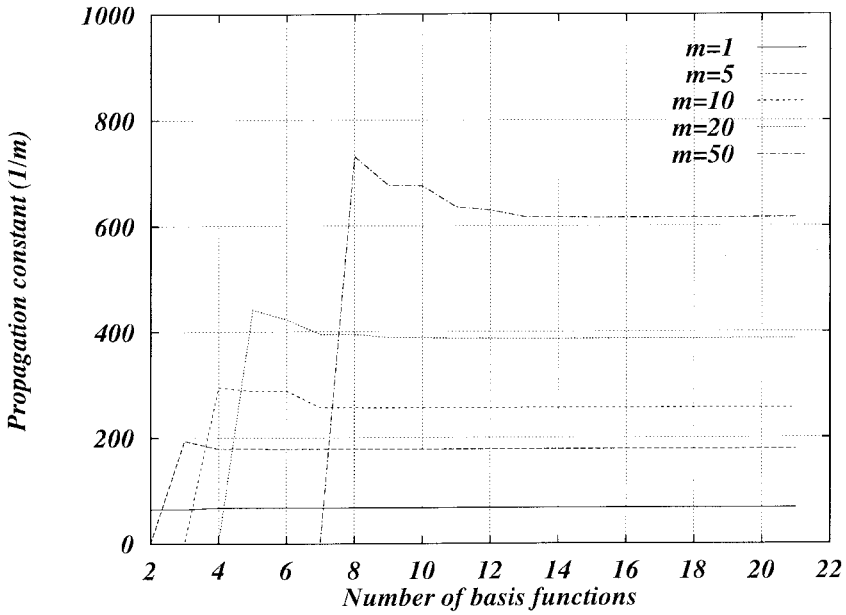

Fig. 3. Convergency of the propagation constant β_m of the mth elliptical mode as a function of the number of basis functions used to describe each mode $N_r = N_s$. ($a = 23.5$ mm, $e = 0.8837$, Frequency = 5 GHz).

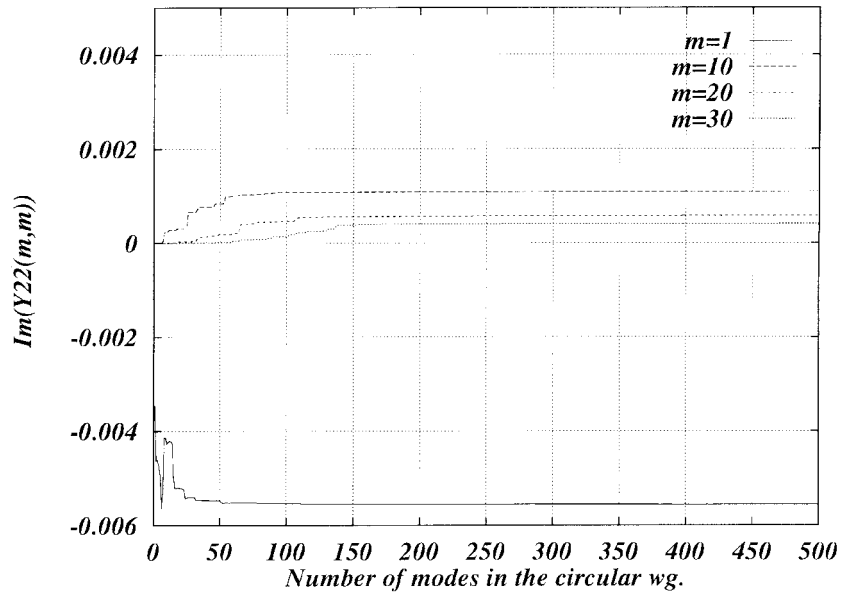

Fig. 4. Convergency of the $Y^{(2,2)}_{m,m}$ element as a function of the number of terms summed in (40) for an elliptical iris in a circular waveguide (frequency = 8.7 GHz).

The elements of the matrices $\underline{\underline{P}}$ and $\underline{\underline{Q}}$ result in

$$Q_{ij}^{\mathrm{TE}_e} = I_{r,t}^{(c3)} \frac{\pi c^2}{\epsilon_s} \delta_{s,p} - I_{s,p}^{(c2)} \frac{c^2 \xi_0}{2\epsilon_r} \delta_{r,t}$$
$$P_{ij}^{\mathrm{TE}_e} = \left[\frac{\pi^3}{\epsilon_s \xi_0} (\epsilon_r - 1)\, rt + \frac{\xi_0 \pi}{\epsilon_r} (\epsilon_s - 1)\, sp \right] \delta_{s,p} \delta_{r,t}$$
$$i \equiv (r,\, s), \quad j \equiv (t,\, p) \tag{29}$$
$$Q_{ij}^{\mathrm{TE}_o} = I_{r,t}^{(s3)} \frac{\pi c^2}{2} \delta_{s,p} - I_{s,p}^{(s2)} \frac{c^2 \xi_0}{4} \delta_{r,t}$$
$$P_{ij}^{\mathrm{TE}_o} = \left[\frac{\pi^3}{2\xi_0} \left(r + \frac{1}{2} \right) \left(t + \frac{1}{2} \right) + \frac{\xi_0 \pi}{2}\, sp \right] \delta_{s,p} \delta_{r,t}$$
$$i \equiv (r,\, s), \quad j \equiv (t,\, p) \tag{30}$$

where the expressions for $I_{r,t}^{(c3)}$ and $I_{r,t}^{(s3)}$ are given in the Appendix.

The scalar potentials $\varphi_m^{\mathrm{TE}_e}$ and $\varphi_m^{\mathrm{TE}_o}$ are written as follows

$$\varphi_m^{\mathrm{TE}_e}(\xi,\, \eta) = \mathcal{N}_m^{\mathrm{TE}_e} \sum_{r=0}^{N_r - 1} \sum_{s=0}^{N_s - 1} d_{rs}^{\mathrm{TE}_e,\,(m)} \cdot \cos\left(r\pi \frac{\xi}{\xi_0} \right) \cos(s\eta) \tag{31}$$

$$\varphi_m^{\mathrm{TE}_o}(\xi,\, \eta) = \mathcal{N}_m^{\mathrm{TE}_o} \sum_{r=0}^{N_r - 1} \sum_{s=1}^{N_s} d_{rs}^{\mathrm{TE}_o,\,(m)} \cdot \sin\left[\left(r + \frac{1}{2} \right) \pi \frac{\xi}{\xi_0} \right] \sin(s\eta) \tag{32}$$

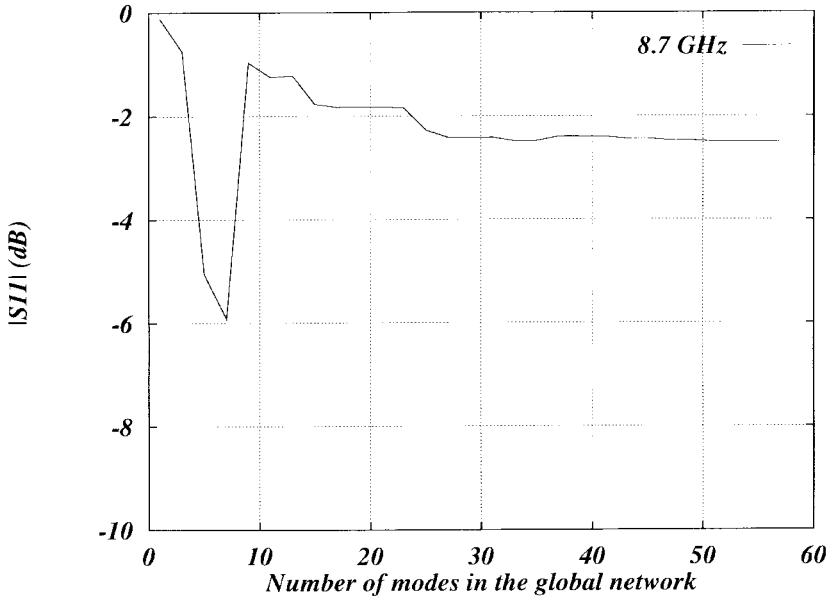

Fig. 5. Convergency of the magnitude of the reflection coefficient versus the number of modes included in the global network for an elliptical iris in a circular waveguide (frequency = 8.7 GHz).

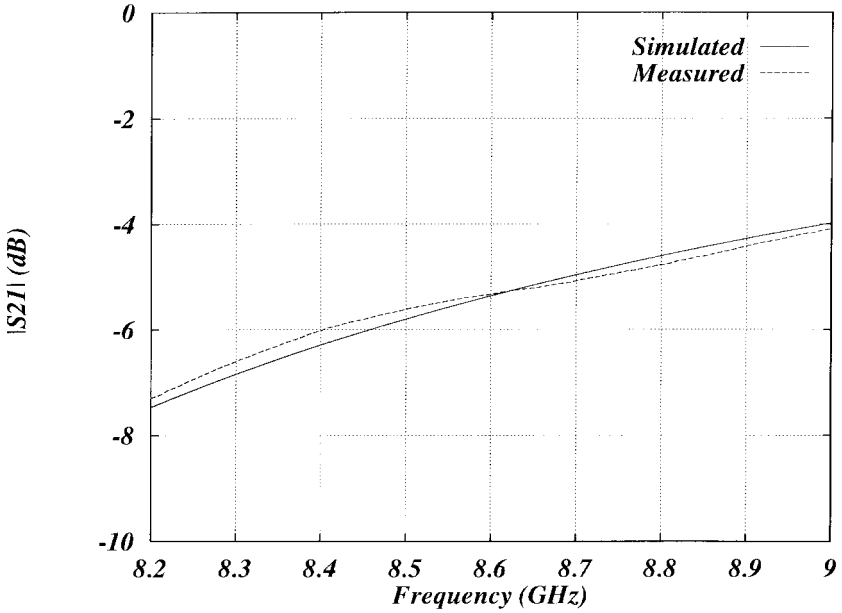

Fig. 6. Comparison between simulation and measurements for an elliptical iris in a circular waveguide.

where $\mathcal{N}_m^{\mathrm{TE}_e}$ and $\mathcal{N}_m^{\mathrm{TE}_o}$, the normalization factors according to the normalization condition (10), are given by

$$\mathcal{N}_m^{\mathrm{TE}_e} = \left\{ \pi \xi_0 \sum_{r=0}^{N_r-1} \sum_{s=0}^{N_s-1} [d_{rs}^{\mathrm{TE}_e,(m)}]^2 \cdot \left[r^2 \frac{1}{\epsilon_s} \left(\frac{\pi}{\xi_0} \right)^2 (\epsilon_r - 1) + s^2 \frac{\epsilon_s - 1}{\epsilon_r} \right] \right\}^{-1/2} \tag{33}$$

$$\mathcal{N}_m^{\mathrm{TE}_o} = \left\{ \frac{\xi_0 \pi}{2} \sum_{r=1}^{N_r} \sum_{s=1}^{N_s} [d_{rs}^{\mathrm{TE}_o,(m)}]^2 \cdot \left[\left(r + \frac{1}{2} \right)^2 \left(\frac{\pi}{\xi_0} \right)^2 + s^2 \right] \right\}^{-1/2} \tag{34}$$

so that the authors can finally write for the TE vector mode functions the following expressions

$$\begin{aligned} \mathbf{h}_m^{\mathrm{TE}_\alpha} &= \nabla_t \varphi_m^{\mathrm{TE}_\alpha} \\ \mathbf{e}_m^{\mathrm{TE}_\alpha} &= \nabla_t \varphi_m^{\mathrm{TE}_\alpha} \times \mathbf{u}_z, \qquad \alpha = e, o \end{aligned} \tag{35}$$

Finally, the modal admittance of the TE modes is given by

$$Y_m^{\mathrm{TE}} = \frac{\beta_m^{\mathrm{TE}}}{\omega \mu} \tag{36}$$

where β_m^{TE} is again the propagation constant given in (2).

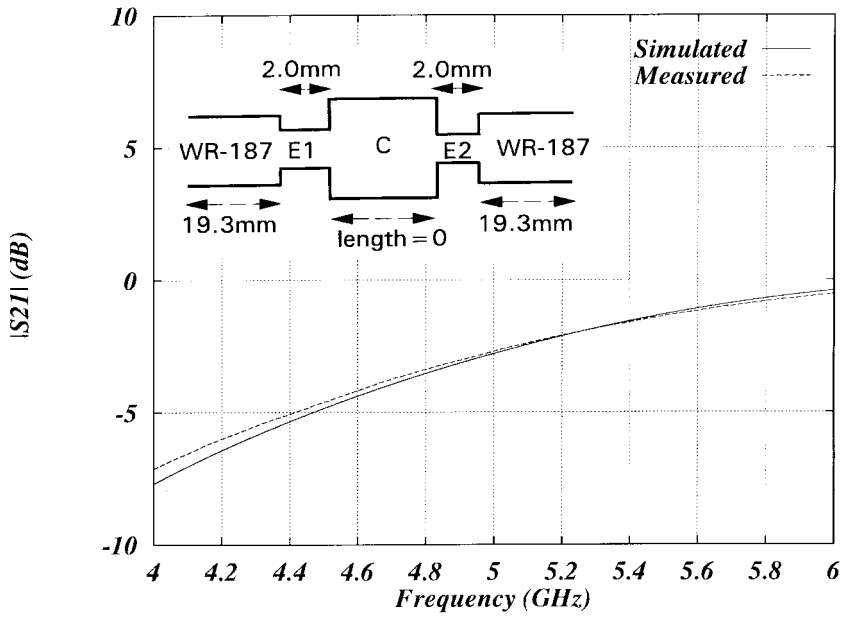

(a)

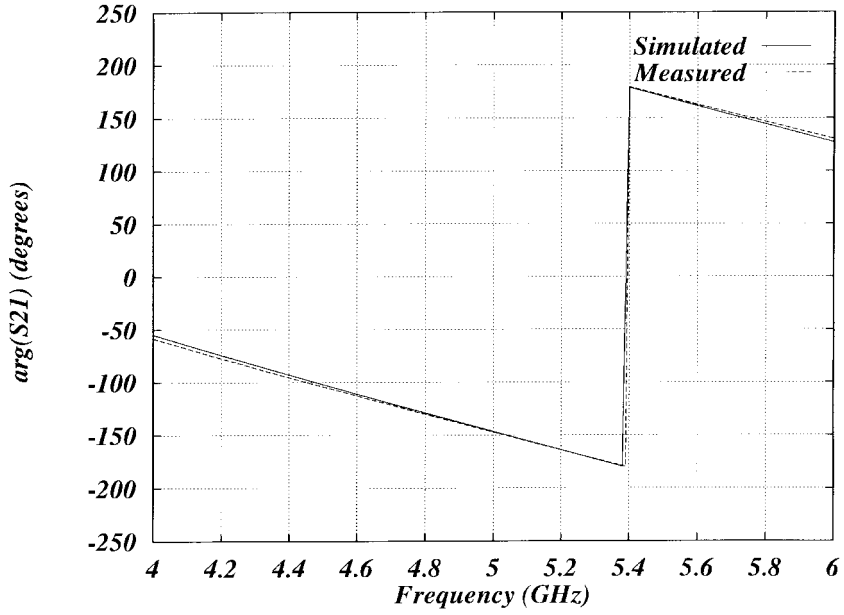

(b)

Fig. 7. Comparison between simulation and measurements for a junction between two elliptical waveguides: (a) magnitude of the transmission coefficient and (b) phase of the transmission coefficient.

III. Junctions Between a Large Waveguide and a Smaller Elliptical Waveguide

Once the modes of the elliptical waveguides have been obtained, the next contribution is the analysis of the discontinuities presented in Fig. 1. To proceed, the authors need to define two reference planes denoted as T and T', as shown in Fig. 2. The plane T' is at the junction between the regions (1) and (2), while the plane T is located at a distance L in the region (1). The authors can then write the mathematical equivalent of the network representation between the reference planes T and T', represented as a multiport in Fig. 2, in the form

$$I_m^{(\delta)} = \sum_{n=1}^{+\infty} Y_{m,n}^{(\delta,1)} V_n^{(1)} + \sum_{n=1}^{+\infty} Y_{m,n}^{(\delta,2)} V_n^{(2)}; (\delta) = (1), (2) \tag{37}$$

where $V_m^{(\delta)}$ and $I_m^{(\delta)}$ are the modal voltages and currents, respectively. Following [17], the authors can now write directly these expressions for the admittance matrix elements,

$$Y_{m,n}^{(1,1)} = -jY_n^{(1)} \cot [\beta_n^{(1)} L] \delta_{m,n} \tag{38}$$

$$Y_{m,n}^{(2,1)} = Y_{n,m}^{(1,2)} = jY_n^{(1)} \operatorname{cosec} [\beta_n^{(1)} L] \langle \mathbf{h}_n^{(1)}, \mathbf{h}_m^{(2)} \rangle \tag{39}$$

$$Y_{m,n}^{(2,2)} = -j \sum_{k=1}^{+\infty} Y_k^{(1)} \cot [\beta_k^{(1)} L] \cdot \langle \mathbf{h}_k^{(1)}, \mathbf{h}_m^{(2)} \rangle \langle \mathbf{h}_k^{(1)}, \mathbf{h}_n^{(2)}. \rangle \tag{40}$$

The problem at hand has therefore been reduced to the evaluation of the inner products between the modes.

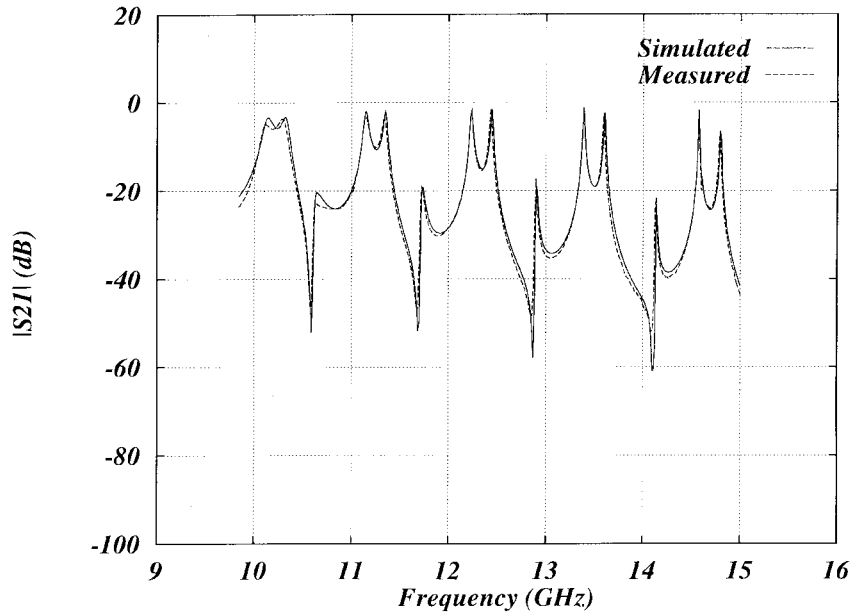

(a)

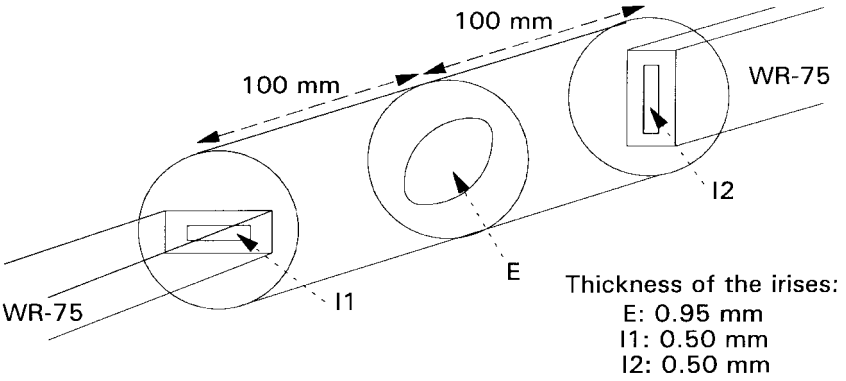

(b)

Fig. 8. (a) Comparison between simulation and measurements for a circular cavity fed by rectangular waveguides. An elliptical iris was inserted in the middle of the cavity. (b) Sketch of the cavity structure.

The inner products involved in (39) and (40) [identified as $\langle \mathbf{h}_n^{(1)}, \mathbf{h}_m^{(2)} \rangle$] are surface integrals which have to be evaluated in the cross section of the ellipse [see (10)]. These surface integrals can be reduced to a simple contour integral [20], obtaining, if n and m refer to TM modes

$$\langle \mathbf{h}_n^{(1)}, \mathbf{h}_m^{(2)} \rangle = \frac{-[k_{t_n}^{(1)}]^2}{[k_{t_m}^{(2)}]^2 - [k_{t_n}^{(1)}]^2} \oint_{\xi=\xi_0} \psi_n^{\mathrm{TM}} \frac{\partial \varphi_m^{\mathrm{TM}_\alpha}}{\partial \xi} \, d\eta; \quad \alpha = e, o \tag{41}$$

if n refers to TM and m refers to TE modes

$$\langle \mathbf{h}_n^{(1)}, \mathbf{h}_m^{(2)} \rangle = - \oint_{\xi=\xi_0} \frac{\partial \psi_n^{\mathrm{TE}}}{\partial \eta} \varphi_m^{\mathrm{TE}_\alpha} \, d\eta; \quad \alpha = e, o \tag{42}$$

if n and m refer to TE modes

$$\langle \mathbf{h}_n^{(1)}, \mathbf{h}_m^{(2)} \rangle = \frac{[k_{t_m}^{(2)}]^2}{[k_{t_m}^{(2)}]^2 - [k_{t_n}^{(1)}]^2} \oint_{\xi=\xi_0} \frac{\partial \psi_n^{\mathrm{TE}}}{\partial \xi} \varphi_m^{\mathrm{TE}_\alpha} \, d\eta; \quad \alpha = e, o \tag{43}$$

if n refers to TE and m refers to TM modes

$$\langle \mathbf{h}_n^{(1)}, \mathbf{h}_m^{(2)} \rangle = 0 \tag{44}$$

where the scalar potentials ψ_n^{TM} and ψ_n^{TE} correspond to the rectangular or circular modes in the region (1) [18].

IV. Accuracy and Convergence Properties of the Modal Expansions

The authors first present in Table I the cutoff wavelengths of several modes for an elliptical waveguide with eccentricity $e = 0.5$ in comparison with [10]. The agreement is very good even for the higher order modes. The computation time for these typical cases is only 167 s on a IBM RISC-6000 workstation ($N_r = N_s = 15$ basis functions were used), while the solution obtained with a program based on a standard package to calculate the Mathieu functions needed 303 s.

Next the authors show in Fig. 3 the convergence of the propagation constant in (2) of several modes as a function of the number of basis functions $N_r = N_s$ used to describe each mode ($e = 0.8837$). The authors can see that the convergence

TABLE I
CUTOFF WAVELENGTHS (CM) OF AN ELLIPSE WITH $2a = 2$ CM, $e = 0.5$

Order	Mode	[10]	This method	Rel. error
1	TE_e	3.39447796	3.39447781	0.4×10^{-5}
5	TE_o	1.90795125	1.90795097	1.5×10^{-5}
10	TE_o	1.39790776	1.39790732	3.1×10^{-5}
20	TE_e	0.91607169	0.91607066	3.1×10^{-5}
30	TM_o	0.77560113	0.77560109	1.1×10^{-4}
50	TM_o	0.59214061	0.5921451	1.7×10^{-5}
70	TM_e	0.49402711	0.49402571	2.8×10^{-4}
90	TM_o	0.43415539	0.43415506	7.6×10^{-5}
100	TE_e	0.41616560	0.41616329	5.6×10^{-4}

of each mode depends on the order of the mode. For instance, to obtain the 50th mode with the accuracy showed in Table I, the authors need to consider at least $N_r = N_s = 15$ basis functions.

V. CASCADING JUNCTIONS

More complicated structures can be easily analyzed by connecting to each other several rectangular, circular and elliptical waveguide lengths. Once the admittance matrices of all of the elements of the structure are evaluated, they can be easily connected to form a global multimode equivalent network. From the network, a band diagonal linear system is obtained, which has to be inverted in order to find the reflection and transmission coefficients at the input and output ports. This inversion is performed by means of an adequate inversion algorithm for band diagonal systems, resulting in a very fast code implementation.

In order to verify the accuracy of the codes developed, several elliptical irises in rectangular and circular waveguides were manufactured with a tolerance of $\pm$ 0.05 mm. The first example consists of an elliptical iris in a circular waveguide with radius $r = 11.7$ mm. The dimensions of the iris were $a = 8$ mm, $b = 5$ mm, and the thickness was 0.95 mm. The iris was tilted of an angle $\theta = 30°$, and was also shifted with respect to the center of the feeding circular waveguide to the point ($r_0 = 2$ mm, $\alpha = 25°$) [see Fig. 1(b)]. In Fig. 4, the authors present the convergence of the element $Y_{m,n}^{(2,2)}$ as a function of the number of terms summed in (40). As the authors can see, 200 terms are enough to reach the region of convergence. The convergence of the reflection coefficient is plotted in Fig. 5 versus the number of modes in the global network. As the authors can see, 40 modes are sufficient to obtain an accurate solution. In Fig. 6, the authors compare our theoretical results with the measurements finding good agreement. To perform all calculations the authors used $N_r = N_s = 10$ basis functions to describe each elliptical mode, 200 terms in (40), 40 modes in the global network and 100 points in frequency. The computation time for the results plotted in Fig. 6 was 2.7 s per point on a IBM RISC-6000 workstation.

The junction between two elliptical guides was also analyzed in this paper [see Fig. 1(c)]. To perform this analysis, instead of applying the method described in Section III, the authors connected the elliptical waveguides through a section of circular waveguide of length zero. In Fig. 7, the authors compare the magnitude and the phase of the transmission coefficient of our theoretical results with the measurements for two centered elliptical irises joined directly showing good agreement. The irises were inserted in WR-187 rectangular waveguide, being their dimensions $a = 20.7$ mm, $b = 8.7$ mm (denoted as E1) and $a = 14.9$, $b = 5.9$ mm (denoted as E2), respectively. The thickness was 2.0 mm for both of them. The radius of the zero length circular waveguide used in the simulation was $r = 25$ mm.

$$I_{r,t}^{(c1)} = \left[\frac{(-1)^{r-t}}{4+(r-t)^2} - \frac{(-1)^{r+t}}{4+(r+t+1)^2}\right]\frac{\xi_0^2 \sinh(2\xi_0)}{\pi^2} \tag{45}$$

$$I_{r,t}^{(s1)} = \left[\frac{(-1)^{r-t}}{4+(r-t)^2} - \frac{(-1)^{r+t}}{4+(r+t)^2}\right]\frac{\xi_0^2 \sinh(2\xi_0)}{\pi^2} \tag{46}$$

$$I_{r,t}^{(c3)} = \left[\frac{(-1)^{r-t}}{4+(r-t)^2} + \frac{(-1)^{r+t}}{4+(r+t)^2}\right]\frac{\xi_0^2 \sinh(2\xi_0)}{\pi^2} \tag{47}$$

$$I_{r,t}^{(s3)} = \left[\frac{(-1)^{r-t}}{4+(r-t)^2} + \frac{(-1)^{r+t}}{4+(r+t+1)^2}\right]\frac{\xi_0^2 \sinh(2\xi_0)}{\pi^2} \tag{48}$$

$$I_{s,p}^{(c2)} = \begin{cases} \text{if } s \neq p \rightarrow \begin{cases} \text{if } p = 0 \text{ or } s = 0 \rightarrow \begin{cases} \pi, & \text{if } s+p = 2 \\ 0, & \text{in other case} \end{cases} \\ \text{if } p \neq 0 \text{ and } s \neq 0 \rightarrow \begin{cases} \dfrac{\pi}{2}, & \text{if } s+p = 2 \text{ or } |s-p| = 2 \\ 0, & \text{in other case} \end{cases} \end{cases} \\ \text{if } s = p \rightarrow \begin{cases} \dfrac{\pi}{2}, & \text{if } s = p = 1 \\ 0, & \text{in other case} \end{cases} \end{cases}$$

$$I_{s,p}^{(s2)} = \begin{cases} \text{if } s \neq p \rightarrow \begin{cases} \dfrac{\pi}{2}, & \text{if } |s-p| = 2 \\ 0, & \text{in other case} \end{cases} \\ \text{if } s = p \rightarrow \begin{cases} -\dfrac{\pi}{2}, & \text{if } s = p = 1 \\ 0, & \text{in other case} \end{cases} \end{cases}$$

Finally, the authors constructed a circular cavity fed from two rectangular waveguides through two rectangular irises. In the middle of the cavity the authors inserted an elliptical iris (denoted as E) with dimensions $a = 9$ mm, $b = 7$ mm, $r_0 = 0$, $\alpha = 0°$, and rotated of $\theta = 45°$. The dimension of the rectangular irises were $a = 18.0$ mm, $b = 1.1$ mm for the first iris (denoted as I1), and $a = 1.1$ mm, $b = 14.1$ mm (denoted as I2) for the second one. The radius of the circular waveguide was $r = 11.7$ mm. The magnitude of the transmission coefficient is plotted in Fig. 8, showing also good agreement.

VI. Conclusions

An accurate multimode equivalent network representation for the junctions between rectangular, circular or elliptical to elliptical waveguides has been developed. The multimode equivalent network representation is formulated in terms of an admittance coupling matrix. Furthermore, a computationally efficient modal expansion for the elliptical waveguide is obtained in terms of a linear matrix eigenvalue problem. The convergence of the method is good. Comparisons between theoretical and experimental results fully validate the network representations developed.

Appendix
Definition of $I_{r,t}^{(c1)}$, $I_{s,p}^{(c2)}$, $I_{r,t}^{(s1)}$, $I_{s,p}^{(s2)}$, $I_{r,t}^{(c3)}$, and $I_{r,t}^{(s3)}$

The expressions for $I_{r,t}^{(c1)}$, $I_{s,p}^{(c2)}$, $I_{r,t}^{(s1)}$, $I_{s,p}^{(s2)}$, $I_{r,t}^{(c3)}$, and $I_{r,t}^{(s3)}$ are given by (45)–(48), as shown at the bottom of the previous page.

Acknowledgment

The authors would like to thank to J. Peces of Antennas Division of ESTEC, and D. Raboso and G. Silgado of the Radio Frequency Division of ESTEC, for their help in connection with the experimental verification.

References

[1] L. J. Chu, "Electromagnetic waves in elliptic hollow pipes of metal," *J. Appl. Phys.*, vol. 9, pp. 583–591, Sept. 1938.
[2] J. P. Kinzer and I. G. Wilson, "Some results on cylindrical cavity resonators," *Bell Syst. Tech. J.*, pp. 423–431, 1947.
[3] R. V. Harrowell, "An approximate theory for determining the characteristic impedances of elliptic waveguide," *J. Elec. Cont.*, vol. 5, pp. 289–299, Oct. 1958.
[4] G. R. Valenzuela, "Impedances of an elliptical waveguide," *IRE Trans. Microwave Theory Tech.*, vol. MTT-8, pp. 431–435, July 1960.
[5] J. G. Kretzschmar, "Cutoff frequency of the TM_{c11} mode in a hollow conducting elliptical waveguide," *Elec. Lett.*, vol. 5, no. 9, pp. 192–193, May 1969.
[6] J. G. Kretzschmar, "Wave propagation in hollow conducting elliptical waveguides," *IEEE Trans. Microwave Theory Tech.*, vol. MTT-18, pp. 547–554, Sept. 1970.
[7] S. B. Rayevskiy and V. Y. Smorgonskiy, "Method of computation of critical frequencies of an elliptical waveguide," *Radio Eng. Elec. Phys.*, vol. 15, no. 9, pp. 1702–1705, 1970.
[8] L. G. Kretzschmar, "Field configuration of the TM_{c01} mode in an elliptical waveguide," *Proc. Inst. Elect. Eng.*, vol. 118, no. 9, pp. 1187–1189, Sept. 1971.
[9] D. A. Goldberg, L. J. Laslett, and R. A. Rimmer, "Modes of elliptical waveguides: A correction," *IEEE Trans. Microwave Theory Tech.*, vol. 38, no. 11, pp. 1603–1608, Nov. 1990.
[10] S. Zhang and Y. Shen, "Eigenmode sequence for an elliptical waveguide with arbitrary ellipticity," *IEEE Trans. Microwave Theory Tech.*, vol. 43, pp. 227–230, Jan. 1995.
[11] J. B. Davies and L. G. Kretzschmar, "Analysis of hollow elliptical waveguides by polygon approximation," *Proc. Inst. Elect. Eng.*, vol. 119, no. 5, pp. 519–522, May 1972.
[12] B. K. Wang, K. Y. Lam, M. S. Leong, and P. S. Kooi, "Elliptical waveguide analysis using improved polynomial approximation," in *IEE Proc. Microwave Ant. Propag.*, vol. 141, no. 6, pp. 483–488, Dec. 1994.
[13] P. Matras, R. Bunger, and F. Arndt, "Mode-matching analysis of the step discontinuity in elliptical waveguides," *IEEE Microwave and Guided Wave Lett.*, vol. 6, pp. 143–145, Mar. 1996.
[14] A. Weisshaar, S. M. Goodnick, and V. K. Tripathi, "A rigorous and efficient method of moments solution for curved waveguide bends," *IEEE Trans. Microwave Theory Tech.*, vol. 40, pp. 2200–2206, Dec. 1992.
[15] D. T. Thomas, "Functional approximations for solving boundary value problems by computer," *IEEE Trans. Microwave Theory Tech.*, vol. MTT-17, no. 8, pp. 447–454, Aug. 1969.
[16] R. M. Bulley, "Analysis of the arbitrarily shaped waveguide by polynomial approximation," *IEEE Trans. Microwave Theory Tech.*, vol. MTT-18, pp. 1022–1028, Dec. 1970.
[17] A. Alvarez and M. Guglielmi, "New simple procedure for the computation of the multimode admittance matrix of planar waveguide junctions," *IEEE Trans. Microwave Theory Tech.*, vol. 44, pp. 413–418, Mar. 1996.
[18] N. Marcuvitz, *Waveguide Handbook.* London, UK: Peter Peregrinus Ltd., 1986.
[19] N. W. McLachlan, *Theory and Application of Mathieu Functions*, First ed. New York: Dover, 1964.
[20] G. G. Gentili, "Properties of TE–TM mode-matching techniques," *IEEE Trans. Microwave Theory Tech.*, vol. 39, pp. 1669–1673, Sept. 1991.

Benito Gimeno received the Licenciado degree in physics and the Ph.D. degree both from the Universidad de Valencia, Spain, in 1987 and 1992, respectively.

He was a Fellow at the Universidad de Valencia from 1987 to 1990. Since 1990, he has been Assistant Professor in the Departmento de Fisica Aplicada at the Universidad de Valencia, where he was teaching and doing research in numerical methods for electromagnetics. He worked at the European Space Research and Technology Centre (ESTEC) of the European Space Agency under a CDTI grant during 1994–1995. His current research interests include the areas of computer-aided techniques for analysis of microwave passive components and waveguide structures.

Marco Guglielmi received the degree "Laurea in Ingegneria Elettronica" in 1979 from the University of Rome "La Sapienza," Rome, Italy, in 1980. He also attended the "Scuola di Specializzazione in Elettromagnetismo Applicato" in the same year. In 1982 he received the M.S. degree in electrical engineering from University of Bridgeport, Bridgeport, CT. In 1986 he received the Ph.D. degree in electrophysics from the Polytechnic University, Brooklyn, NY.

He was Academic Associate at Polytechnic University from 1984 to 1986, and became Assistant Professor in 1986. During 1988–1989, he was an Assistant Professor at the New Jersey Institute of Technology, Newark, NJ. Since 1989, he has been with the RF System Division of the European Space Research and Technology Centre, Noordwijk, The Netherlands, where he is currently involved in the development of passive microwave components for space applications. His research interests include the areas of solid-state devices and circuits, periodic structures, phased arrays and millimeter-wave leaky-wave antennas, network representations of waveguide discontinuities, and microwave filtering structures.